

RSC Advances



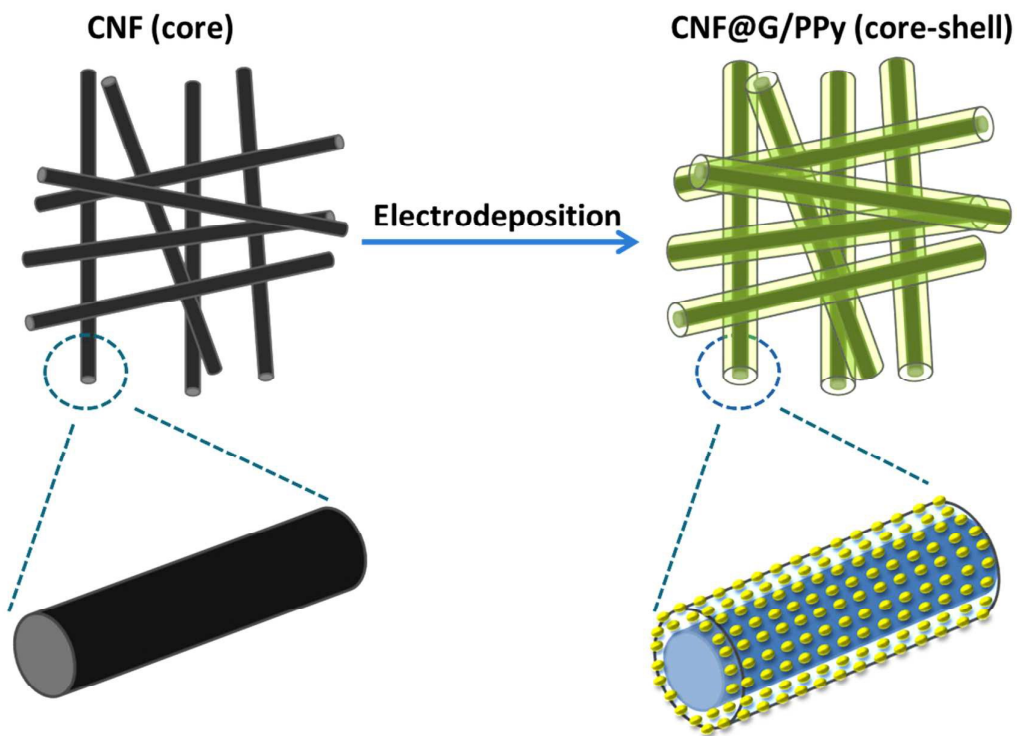
This is an *Accepted Manuscript*, which has been through the Royal Society of Chemistry peer review process and has been accepted for publication.

Accepted Manuscripts are published online shortly after acceptance, before technical editing, formatting and proof reading. Using this free service, authors can make their results available to the community, in citable form, before we publish the edited article. This *Accepted Manuscript* will be replaced by the edited, formatted and paginated article as soon as this is available.

You can find more information about *Accepted Manuscripts* in the [Information for Authors](#).

Please note that technical editing may introduce minor changes to the text and/or graphics, which may alter content. The journal's standard [Terms & Conditions](#) and the [Ethical guidelines](#) still apply. In no event shall the Royal Society of Chemistry be held responsible for any errors or omissions in this *Accepted Manuscript* or any consequences arising from the use of any information it contains.

Graphical Abstract



In this study, a two-step electrospinning and potentiostatic electrodeposition method was used to fabricate the graphene/polypyrrole-coated carbon nanofibers core-shell architecture electrode for supercapacitor applications.

Graphene/polypyrrole-coated carbon nanofibers core-shell architecture electrode for electrochemical capacitors

John Kevin Gan,¹ Yee Seng Lim,¹ Alagarsamy Pandikumar,^{1*} Nay Ming Huang,^{1*}
Hong Ngee Lim^{2,3*}

¹ Low Dimensional Materials Research Centre, Department of Physics, Faculty of Science,
University of Malaya, 50603 Kuala Lumpur, Malaysia

² Department of Chemistry, Faculty of Science, Universiti Putra Malaysia,
43400 UPM Serdang, Selangor, Malaysia

³ Functional Device Laboratory, Institute of Advanced Technology, Universiti Putra Malaysia,
43400 UPM Serdang, Selangor, Malaysia

Corresponding authors: huangnayming@um.edu.my (Huang N.M.),
janet_limhn@science.upm.edu.my (Lim H.N.) and
pandikumarinbox@gmail.com (Pandikumar. A)

Abstract

Herein we report a two-step electrospinning and potentiostatic electrodeposition method to fabricate electrodes with graphene/polypyrrole-coated carbon nanofibers core-shell architecture for supercapacitor applications. The electrospun carbon nanofibers core acts as an electrically conductive substrate that enables the incorporation of the graphene/polypyrrole shell. Constructing a porous and interconnected one-dimensional configuration with a carbon nanofibers core, facilitates the maximum electrochemical utilization of the graphene/polypyrrole shell. The addition of graphene significantly decreases the charge transfer resistance of the electrode by reducing the distance for electron shuttling in the polypyrrole chains for rapid electrochemical redox reactions. As a consequence, the specific capacitance of the core-shell electrode was enhanced up to 386 F/g at 2 mV/s. The enhanced conductivity and improved stability of the core-shell composite electrode is able to retain 84% of its initial capacitance value over 1000 charge/discharge cycle. The excellent electrochemical performance demonstrates that electrodes with graphene/polypyrrole-coated carbon nanofiber core-shell architecture have great potential for electrochemical energy conversion and storage devices.

1. Introduction

The rapid depletion of fossil fuels has led to the increasing demands for renewable energy sources and has shifted the focus of the scientific community toward the development of energy conversion and storage devices.¹ Electrochemical capacitors, or supercapacitors, appear to offer great promise as energy storage devices with a high power density, excellent reversibility and high cycling stability.² Energy is stored in a supercapacitor by means of capacitive, pseudocapacitive or a combination of the two types. Electric double-layer capacitors (EDLCs) are capacitive in nature where charges are stored electrostatically by the adsorption of ions at the highly accessible specific surface area of the electrode/electrolyte interface.³ In contrast, a pseudocapacitor stores charges faradaically relying on the rapid and reversible redox reactions that occur at the surface of the active material of the electrodes.⁴

Carbonaceous materials such as activated carbons, carbon nanotubes, and graphene are often used as EDLCs because of their excellent conductivity and long life-cycles. However, these materials have low specific capacitance values (5-200 F/g).⁵ Among all the carbon based nanomaterials, graphene has attracted the interest of researchers because of its high theoretical surface area that reaches up to 2630 m²/g for a single graphene sheet, as well as its high electrical conductivity (10⁶ S/cm) making it an attractive candidate for use in electrochemical capacitors.⁶⁻⁸ Conducting polymers such as polyaniline, polypyrrole (PPy), and polythiophene are pseudocapacitive in nature and they have relatively higher capacitances compared to carbon-based materials. PPy, which has a conjugated structure of C=C double bonds, is a promising candidate for pseudocapacitor due to its high electrical conductivity and easy electrochemical processability compared to other conducting polymers.^{9,10} However, like most conducting polymers, the setback of PPy is that it suffers from low mechanical stability and a shorter life cycle due to phase changes and the slow diffusion of ions within the bulk of the electrode during faradic reaction¹¹. To improve the utilization of PPy, it has been strategically combined with carbon-based materials by preparing

PPy/carbon nanotube,^{9,12} PPy/carbon aerogel,¹³ PPy/activated carbon,¹⁴ PPy/porous carbon fiber paper,¹⁵ and PPy/vapour grown carbon fibers.¹⁶

Although not a conducting polymer like PPy, polyacrylonitrile (PAN) is widely used as a precursor in the preparation of carbon nanofibers (CNF) because of its high carbon yield and flexibility. Furthermore, a viscous PAN solution can be stretched easily under a high electrical voltage into fine filaments during electrospinning, which is a simple and convenient method that has been utilized in the preparation of many polymer fibers with diameters ranging from tens of nanometers to several micrometers from polymer solutions.¹⁷ It is a relatively simple and low-cost method for forming continuous, non-woven nanofibers.¹⁸⁻²⁰ Electrospun CNF is interesting due to its high specific surface area and porosity, reasonable electrical conducting framework and good interconnectivity. The porous web structure provides a good supporting network for the incorporation of active electrode materials and its pore accessibility enables rapid intercalation/deintercalation of electrolyte made it an interesting substrate material for promising use in supercapacitor.^{21,22}

Recently, Liu et al. prepared graphene/PPy composite via two-step method involving in situ oxidative polymerization of PPy in aqueous graphene oxide (GO) followed by chemical reduction of the GO.²³ The powdered composite requires the use of insulating binder in the fabrication of electrode that would disrupt the electron transport of the electrode.^{21,24} Electropolymerization of Graphene/PPy composite is a useful technique to eliminate the use of binder where active materials can be directly grown on a freestanding substrate such as platinum²⁵ and tantalum sheet.²⁶ However, the limited area and flat surface of the substrate are unable to support the growth of active materials lead to thick coating and contribute to inactive mass, substantially reducing the specific capacitance of the electrode. In the present work, we combined the benefits of electropolymerization techniques with the benefits of CNF as a conductive substrate. Graphene/PPy (G/PPy) composite was grown directly on electrospun CNF for the first time to produce a unique core-shell structure for high-

performance electrochemical capacitors. The improved capacitance and rate-capability of G/PPy electrodes can be attributed to several aspects, including that (1) The interwoven and porous structure of the electrospun CNF improves the electrolyte accessibility, results in maximum utilization of active materials; (2) the incorporation of graphene into the PPy matrix enhances the performance of the electrode by effectively improving the conductivity and reducing the charge transfer resistance of the electrode; (3) the unique core-shell structure without the need of a binder effectively enhances the interfacial charge transfer. Benefiting from these features, the graphene/PPy grown on CNF is shown to exhibit significantly improved electrochemical performance.

2. Experimental Methods

2.1 Materials

Polyacrylonitrile (PAN, MW: 150,000 g/mol) was obtained from Sigma-Aldrich. Sodium sulfate (Na_2SO_4 , 99 %) and N,N-dimethylformamide (DMF, 99.5 %) were purchased from System. Sodium p-toluenesulfonate (NapTS, 98 %) was purchased from Merck. Pyrrole (99 %) was purchased from Acros Organic and was stored at 0 °C and distilled prior to use. Deionized water was used throughout the sample preparation.

2.2 Fabrication of CNF electrode

The CNF electrode was fabricated by using an electrospinning method, followed by a carbonization process. A 10 wt. % solution of PAN was prepared by dissolving PAN powder in DMF at 80 °C under stirring. After cooling to room temperature, the PAN/DMF solution was loaded into a 10-mL syringe connected to a metal spinneret. Nanofibers were formed by applying 11 kV between the metal spinneret and the grounded rotating mandrel. The feeding rate for the polymeric solution was 1.5 mL/h and the needle-to-collector distance was fixed at 10 cm. The as-spun nanofiber films were peeled off from the collector and dried overnight in an oven at 80 °C. The stabilization and

carbonization of the nanofiber films were carried out in a tubular quartz furnace. The electrospun PAN nanofibers were heated from room temperature to 280 °C at a heating rate of 1 °C/min and maintained at this temperature for 1 h for the oxidative stabilization of PAN. Finally a CNF electrode was obtained by the carbonization of the stabilized PAN nanofibers at 850 °C for 1 h with a heating rate of 5 °C/min in a N₂ atmosphere.

2.3 Fabrication of CNF@G/PPy core-shell electrode

The CNF@G/PPy core-shell electrode was fabricated as follows. The G/PPy was coated on the CNF using a three electrode setup, where the conductive CNF was used as the working electrode, a saturated calomel electrode (SCE) was used as the reference electrode, and a platinum wire served the counter electrode. A piece of CNF film was immersed into an aqueous solution containing 1 mg/mL graphene oxide (modified Hummer's method),²⁷ 0.1 M NapTS and pyrrole monomer (0.1 to 0.3 M) and a constant bias of +0.8V (versus SCE) was applied for 30 min. After the electrodeposition, the CNF@G/PPy core-shell electrodes were washed with copious amounts of DI water to remove the excessive electrolyte. Finally the each sample was dried overnight in an oven at 40 °C and denoted as CNF@G/PPy-xM where x depicts the concentration of the pyrrole monomer used for the deposition. The mass of the graphene/PPy deposited was estimated by weighing the CNF substrate before and after deposition. For comparison, electrodeposition was carried out without the presence of graphene oxide (GO) and was labelled CNF@PPy. The mass of deposited material was comprised between 1.2 – 1.5 mg/cm².

2.4 Structural characterization and electrochemical measurements

The morphologies of the fabricated CNF@G/PPy core-shell electrodes were examined using JEOL JSM-7600F field emission scanning electron microscope and JEOL JEM-2100F high-resolution transmission electron microscope. The Fourier transform infrared (FTIR) spectra were recorded on a Perkin-Elmer FT-IR spectroscopy model 1725x and the Raman spectra were measured using a Reinshaw inVia Raman microscope with green laser excitation (532 nm). The electrochemical

properties of the CNF@G/PPy core-shell electrodes were investigated using Gamry Reference 600. All of the electrochemical measurements were carried out using a three-electrode configuration in 0.5 M Na₂SO₄ electrolyte. Each as-prepared core-shell electrodes was used directly as a working electrode, with Pt and SCE as the counter and reference electrodes, respectively. Cyclic voltammetry (CV) and galvanostatic charge/discharge (GCD) operations were conducted to evaluate the electrochemical performances of the samples. The specific capacitance was calculated from the CV and GCD curves using equations (1) and (2), respectively.

$$C = \frac{1}{mv\Delta V} \int i(V)dV \quad (1)$$

$$C = \frac{I\Delta t}{m\Delta U} \quad (2)$$

where C is the specific capacitance, m is the mass of the active materials in the electrode, v is the potential scan rate, ΔV is the potential window in the CV, $\int i(V)dV$ is the integrated area of the CV curve, I is the discharge current, Δt is discharge time and ΔU is the potential window in the discharge curve. The energy and power density were calculated from the GCD measurements by employing the equations (3) and (4), respectively.

$$E = \frac{1}{2}CV^2 \quad (3)$$

$$P = E/\Delta t \quad (4)$$

where E is the energy density, C is the specific capacitance, V is the working potential window, P is the power density and Δt is the discharge time. Electrochemical impedance spectroscopy (EIS) was carried out with a perturbation amplitude of 5 mV versus the open-circuit potential within a frequency range of 100 kHz to 20 mHz.

3. Results and Discussion

3.1 Material characterization

The G/PPy composite was coated on the surface of the electrospun CNF via a facile and easily scalable electrodeposition method. The CNF offers a well-interconnected conductive framework that is very suitable for anchoring capacitive materials. During the electrodeposition process, GO was reduced and pyrrole was simultaneously electropolymerized to PPy. This produced a uniform coating of G/PPy composite on the CNF surface, which formed a core-shell structure, as illustrated in Fig. 1. The electrochemical reduction of GO to graphene from aqueous suspension had been reported by applying reduction voltages between -1.0 to -1.2 V,²⁸ however, pyrrole monomers are unable to polymerize at negative potentials. We found that the deposition of graphene from GO solution at positive potentials is only possible in the presence of pyrrole monomer. The formation mechanism of G/PPy composite had been explained in detail by Lim et al.²⁹ During the initial stage of electropolymerization of pyrrole, oxidation of monomer occur at the surface of the electrode to form the radical cations of pyrrole monomer while releasing free electrons in the process. The coupling process between two cation radicals followed by the expelling of two protons result in an aromatic dimer. The electro-oxidation of dimer into a cation radical enables it to undergo coupling process to form oligomers. The propagation step continues via oxidation, coupling, deprotonation process until the final product is obtained.³⁰ The negatively charged GO will be attracted to the oligomer radical cations due to electrostatic charge attraction and subsequently reduced to graphene by the free electrons released upon the formation of radicals. The formation of the PPy chain proceeds simultaneously with the reduction of GO, resulting in the embedment of graphene into PPy matrix through π - π stacking and Van der Waals forces. The reduction of GO by pyrrole via chemical method where pyrrole acts as a reducing agent has also been reported elsewhere.³¹

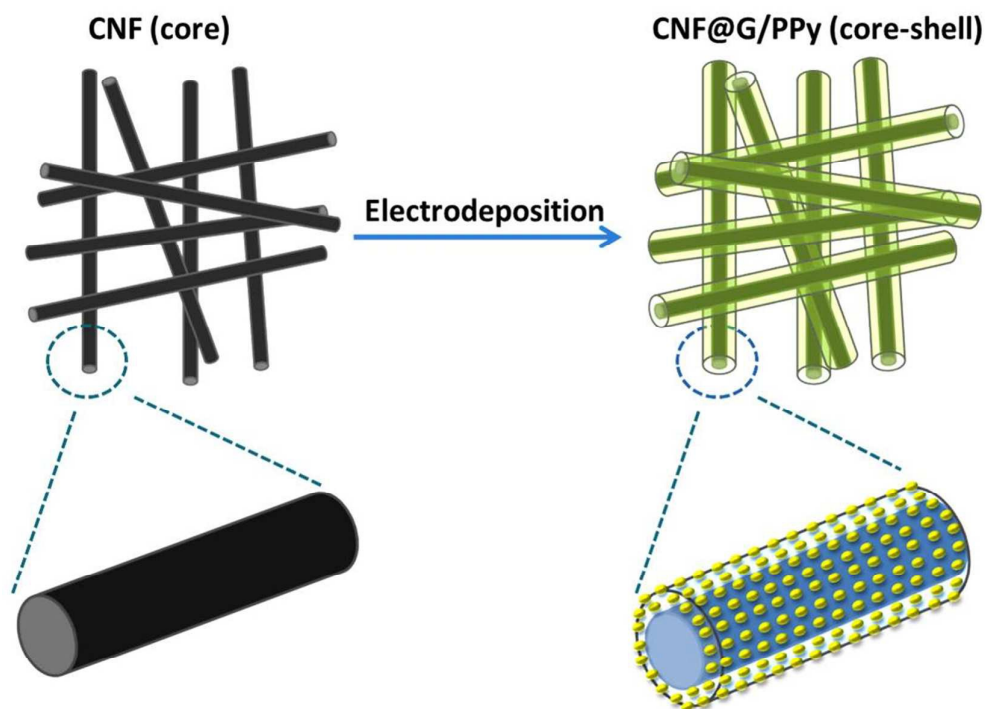


Fig. 1 Schematic illustration of the formation of the core-shell structure.

Fig. 2a and the inset show the FESEM images of the interconnected CNF, which had a smooth surface with an average diameter of 370 nm. Fig. 2b-e shows FESEM images of the G/PPy coated CNF core-shell structure and it shows the increase in the diameter, which ranged from 490 nm to 590 nm after electrodeposition. At 0.1 M of the pyrrole monomer, the folds in the edges of graphene sheets can be clearly seen on the nanofiber surface due to the low ratio of PPy, as shown by Fig. 2b. In the case of 0.2 M, the grown PPy appears to be more protruded and bulbous compared to its appearance at the higher concentration of 0.3 M, where the PPy tends to agglomerate on the surface of the graphene. As can be seen from Fig. 2e, in the absence of graphene, the CNF@PPy shows a PPy growth in the form of flakes on the CNF surface. It is known that the presence of oxidized defects in the graphene supports the nucleation of new polymer chains.^{32,33} Without graphene, the continuous growth of polymer chains causes an increase in the particle density and surface coverage of the nanofibers. Elemental mapping was performed for the

CNF@G/PPy core-shell structure, as shown in Fig. 2f. The areas of bright contrast correlates to the distributions of C and N atoms in the fibers.

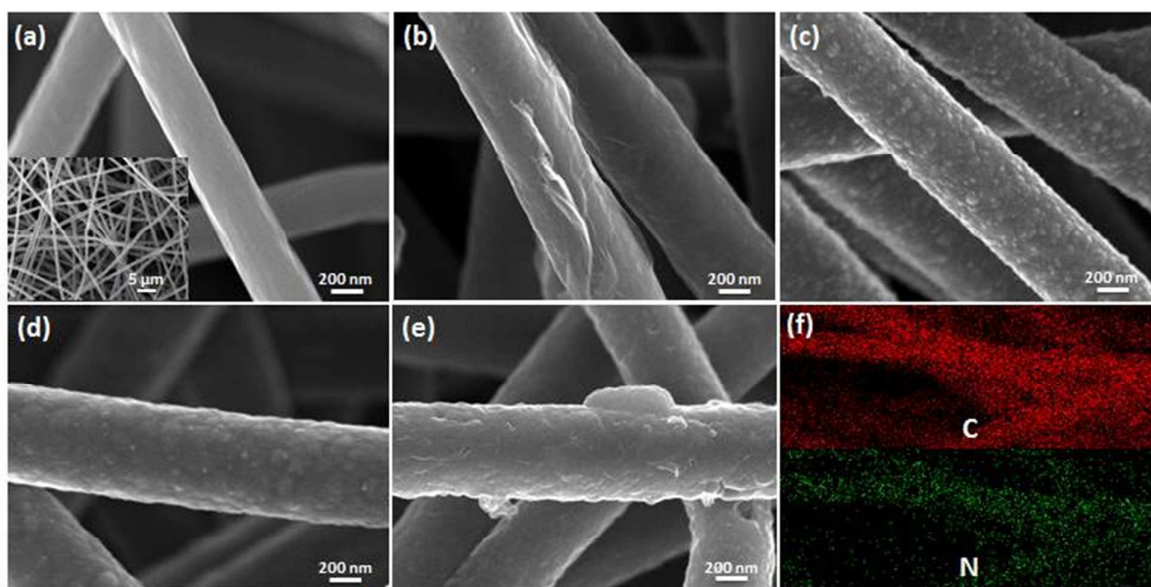


Fig. 2 FESEM images of (a) CNF, with inset showing CNF at lower magnification, (b-d) CNF@G/PPy core-shell with pyrrole concentration from 0.1 M to 0.3 M respectively, (e) CNF@PPy, and (f) elemental mapping of CNF@G/PPy core-shell with 0.2 M pyrrole monomer.

HRTEM images of the CNF and CNF@G/PPy core-shell fibers are shown in Fig. 3. A clear distinction can be observed between the coated and uncoated CNF. Fig. 3a shows the CNF without any coating, which will serve as a conductive backbone with good structural continuity for the coating of G/PPy composites. The G/PPy electrochemically deposited on the CNF surface is shown in Fig. 3b, where the white spots seen in the fiber correspond to the PPy embedded in the graphene matrix. Fig. 3c shows the G/PPy shell uniformly wrapped around a strand of the CNF core to form a unique core-shell structure with increased diameter. From the FESEM and HRTEM analyses, the addition of graphene formed a flexible and homogenous sheet with PPy to wrap around the CNF.

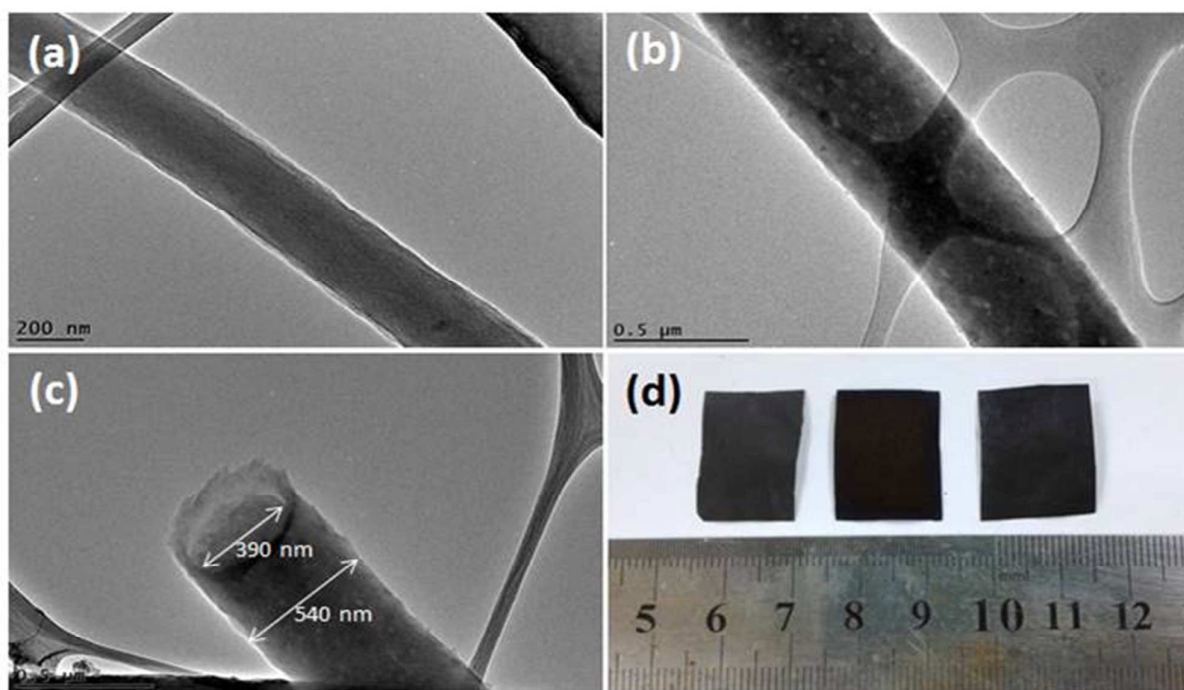


Fig. 3 HRTEM images of (a) bare CNF, (b) CNF@G/PPy along fiber network, (c) CNF@G/PPy at edge of fiber, and (d) photograph of as-prepared bare CNF, CNF@PPy, and CNF@G/PPy from left to right.

Fig. 4a shows the FTIR spectra of GO, CNF, CNF@G/PPy and CNF@PPy. The GO shows peaks at 1728, 1623, 1219, and 1042 cm^{-1} , which are attributed to the stretching vibrations of the C=O carboxyl groups, aromatic C=C, C-OH, and C-O, respectively.³⁴ In the case of CNF, the peak at 1678 cm^{-1} corresponds to the C=C stretching vibration. For CNF@G/PPy and CNF@PPy, the characteristics PPy peaks at 1569 and 1467 cm^{-1} are associated with the C-C and C-N stretching of the PPy rings. The breathing vibration of the pyrrole ring was exhibited at 1211 cm^{-1} , and the band at 1040 cm^{-1} was assigned to the =C-H in-plane vibration. A weak peak at 1083 cm^{-1} was contributed by the in-plane deformation vibration of NH^+ groups, which came from the protonation of the PPy chains.³⁵ The bands at 960 and 915 cm^{-1} can be ascribed to the C-C out-of-plane and C-H out-of-plane vibrations of the PPy rings, respectively. In the CNF@GPPy, the peak of the C=O

stretching vibration of the carboxyl disappeared, indicating that the reduction of the GO was achieved.³⁶

Raman spectra of GO, CNF, CNF@G/PPy and CNF@PPy are shown in Fig. 4b. The GO exhibits the typical D band at 1350 cm^{-1} due to the defects and in-plane terminations of amorphous carbon films, while the G band at 1597 cm^{-1} corresponds to the vibration of sp^2 -bonded carbon atoms in a 2-D hexagonal lattice.²⁵ The intensity ratio of the D and G bands (I_D/I_G) reflects the extent of disordered graphite. The I_D/I_G for GO is calculated to be 0.97, indicating the exfoliation of GO and the presence of oxide functional groups on the basal planes and edges of the GO sheets.³⁷ The peaks observed for CNF at 1348 and 1588 cm^{-1} are in good agreement with the well-documented D and G bands, respectively. For the CNF@PPy, the characteristic peaks at 1352 and 1572 cm^{-1} are assigned to the ring stretching mode and C=C backbone stretching of PPy, respectively. The peaks at 976 and 1076 cm^{-1} were due to the polaron structure and symmetric C-H in-plane bending vibration, respectively.³⁸ The characteristic absorption peaks of PPy are also exhibited in CNF@G/PPy with little alteration to the bands, which indicates the presence of the unchanged internal structure of PPy in the composite.

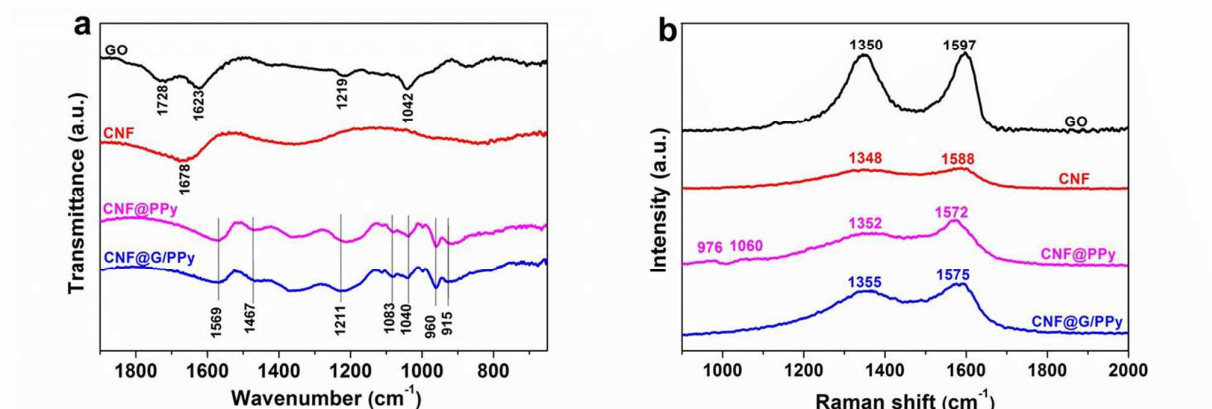


Fig. 4 (a) FTIR and (b) Raman spectra of GO, CNF, CNF@PPy, and CNF@G/PPy.

3.2 Electrochemical characterization

Cyclic voltammogram (CV) technique was used to evaluate the electrochemical performances of the CNF, CNF@PPy, and CNF@G/PPy core-shell electrodes. Fig. 5a shows the

CV curves obtained for the different electrodes at scan rate of 10 mV/s with 0.5 M Na₂SO₄ as the electrolyte. It is apparent that the peak current density was greatly enhanced for both electrodes (CNF@PPy and CNF@G/PPy core-shell) compared to the uncoated CNF electrode, and CNF@G/PPy core-shell electrode showed the maximum current density. Moreover, the CNF@G/PPy core-shell electrode exhibited a good rectangular and symmetrical shape, whereas the CNF@PPy showed a slightly distorted rectangular shape, which suggested good capacitive behavior for the CNF@G/PPy core-shell electrode. The specific capacitances for different electrodes were calculated from the CV curves using equation 1 at 2 mV/s. A capacitance of 6 F/g was found for bare CNF which is in good agreement with the reported literatures.^{24,39,40} This is due to the limited electro-active sites and also small specific surface area of the CNF (17 - 31 m²/g).^{39,41,42} Moreover, in the case of the composites, most of the CNF can barely involve in the charge-storage process that occurs on the surface or near-surface because it has been shielded by the uniform coating of G/PPy composite. Therefore the contribution of the bare CNF substrate to the overall contribution to the composite electrodes is negligible. The specific capacitance was calculated based on the mass of active materials deposited onto the CNF at 2 mV/s, and the value jumped to 265 F/g for the CNF@PPy electrode. Further, the specific capacitance value increased to 386 F/g with the incorporation of graphene with PPy on the CNF surface for the CNF@G/PPy core-shell electrode, which was almost a 46 % increase compared to that for the CNF@PPy electrode. The nucleation of new PPy chains supported by the graphene gave rise to the bulbous structure of the PPy (Fig. 2c), which provided a large surface area for the rapid penetration of the electrolyte. The notable improvement when graphene was added demonstrates the improved conductivity of the G/PPy composite, whereby the inclusion of graphene in the PPy film is able to facilitate the charge transportation within the electrode.⁴³ Although the specific capacitance of the uncoated CNF substrate seems trivial by comparison, it plays a huge role by offering a conductive network for efficient electron transport to the active materials. By taking advantage of the porous structure and high surface area of the CNF, the G/PPy composite can be coated on the surface, where it can be

fully utilized as a result of better access to the electrolyte ions.⁴⁴ The influence of the scan rate on the specific capacitance of the CNF@G/PPy core-shell electrode is shown in Fig. 5b. The slightly distorted rectangle shape at 100 mV/s is due largely to the lesser charge mobilization per unit time of the electrolyte to the interior surfaces of the active materials at a high scan rate.⁴⁵ Hence, increasing the scan rate would lead to gradual decrease in the specific capacitance.

The effect of the concentration of the pyrrole monomer used during electrodeposition was further investigated. Fig. 5c shows that the G/PPy prepared with 0.2 M of pyrrole had the largest area in the CV curves compared to those of 0.1 M and 0.3 M. The specific capacitances of the G/PPy composites are 333, 386, and 291 F/g, when respective concentrations of 0.1, 0.2, and 0.3 M of pyrrole were used in the fabrication of the CNF@G/PPy core-shell electrodes. Decreasing the concentration of pyrrole also decreased the specific capacitance as a result of a smaller contribution of Faradic reactions by PPy. When the concentration of pyrrole was increased to 0.3 M the specific capacitance of the composite dropped to 291 F/g, because of the agglomerates of the PPy in the composite, as confirmed by FESEM. These results indicate that improved electrochemical properties of G/PPy will only be manifested with an appropriate ratio of graphene to PPy, highlighting the importance of finding the optimum concentration for the monomer.

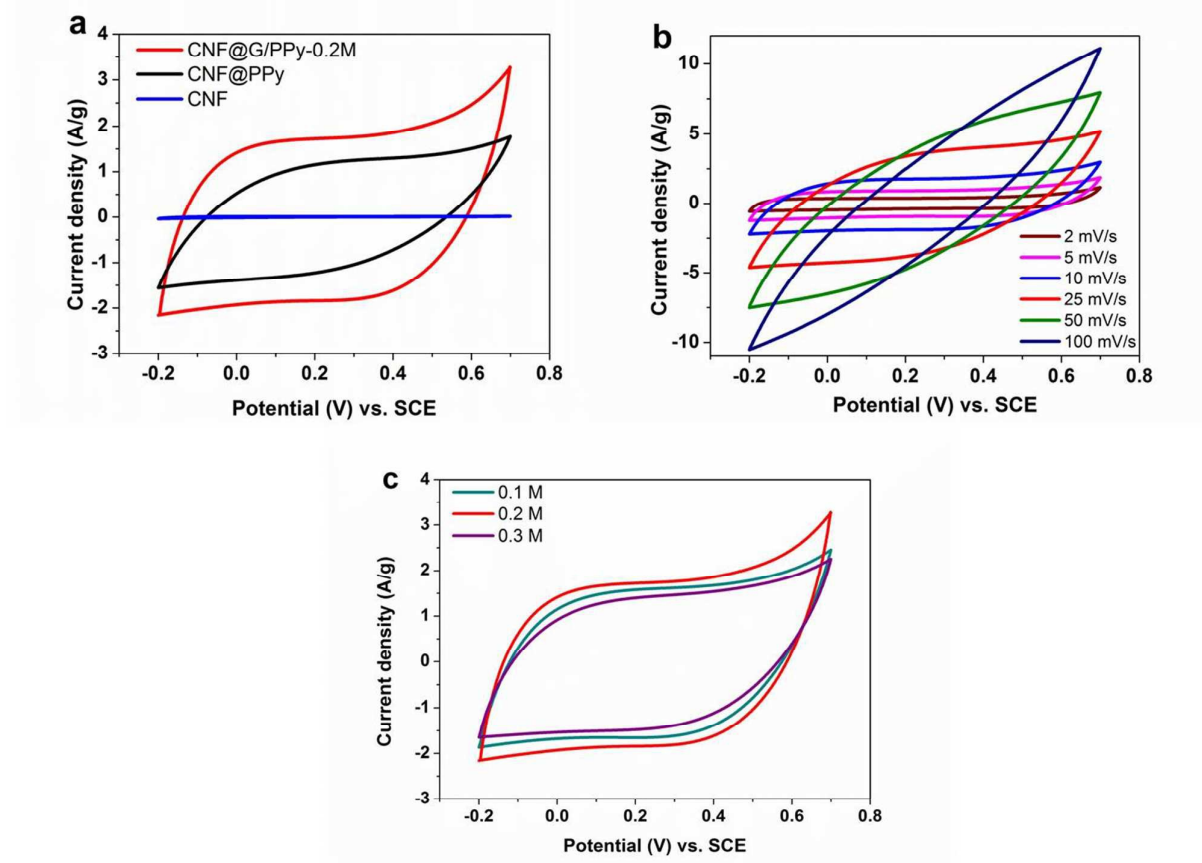


Fig. 5 (a) CV curves obtained for CNF@G/PPy, CNF@PPy and CNF, at scan rate of 10 mV/s, (b) CV curves obtained for CNF@G/PPy core-shell electrode at different scan rates, and (c) CV curves obtained for CNF@G/PPy core-shell electrodes with different concentration of pyrrole monomer at scan rate of 10 mV/s.

Galvanostatic charge/discharge (GCD) operations were employed to further study the electrochemical properties of the CNF@G/PPy core-shell electrodes. The specific capacitances of the CNF@PPy and CNF@G/PPy core-shell electrodes prepared with different concentrations of pyrrole at different current densities were investigated and are summarized in Fig. 6a. The specific capacitances were calculated at a current density of 1 A/g using equation 2, and the values were found to be 258, 325, 380, and 286 F/g for the CNF@PPy electrode and the CNF@G/PPy electrodes fabricated with 0.1, 0.2, and 0.3 M of the pyrrole monomer, respectively. The observed

specific capacitance values were in good agreement with the CV results. The specific capacitance of the CNF@G/PPy-0.2M electrode at 10 A/g remained high at 238 F/g, with capacitance retention of 63%. However, for the CNF@G/PPy-0.3M and CNF@PPy, their specific capacitances decreased drastically to 39 F/g and 11 F/g, respectively, and only 4% of the capacitance was retained for the graphene-free electrode. Without graphene, the PPy's drawback of slow diffusion of ions becomes more significant because of the shortened diffusion time at high current densities.¹¹ The internal resistance (IR) drop observed in the CNF@G/PPy electrode was obviously smaller than that of the CNF@PPy electrode, as shown in Fig. 6b. This demonstrated that the CNF@G/PPy electrode has a low contact resistance upon the initial charge-discharge switch.

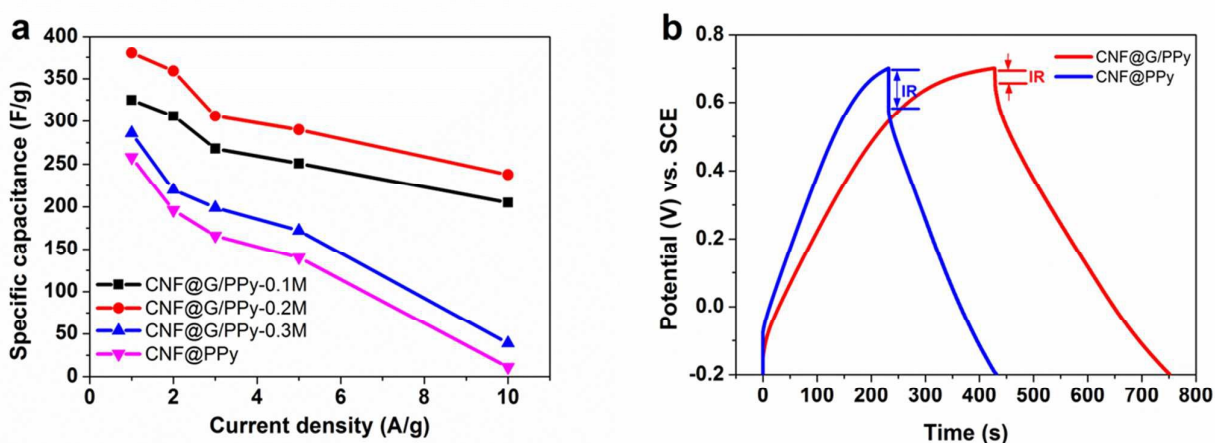


Fig. 6 (a) Dependence of specific capacitance on current density for CNF@PPy and CNF@G/PPy core-shell electrodes, (b) galvanostatic charge/discharge curves obtained for the CNF@PPy and CNF@G/PPy core-shell electrodes at current density of 1 A/g.

The galvanostatic charge/discharge curves of CNF@G/PPy (Fig. 7) at various current densities showed that the charging slope is almost symmetric to their corresponding discharging slopes counterparts. This desirable feature of the electrode indicates an excellent electrochemical reversibility, allowing it to operate at a wide range of current densities. Fig S1 shows the cycle performance of the core-shell electrodes measured at current densities of 2 A/g for 1000 cycles. The

CNF@G/PPy electrode exhibits good long-term cycling stability, retaining 84% of its initial capacitance after 1000 cycles, while only 70% of capacitance retention for CNF@PPy electrode. These results demonstrated that the addition of graphene is able to enhance the cycling stability of PPy. The Ragone plot for the CNF@G/PPy core-shell electrode is shown in Fig. S2. It shows the energy density of the electrode decreases from 38.0 to 10.5 Wh/kg as the power density increases from 424.5 to 2820 W/kg. The maximum power density of 2820 W/kg was obtained with an energy density of 10.5 Wh/kg.

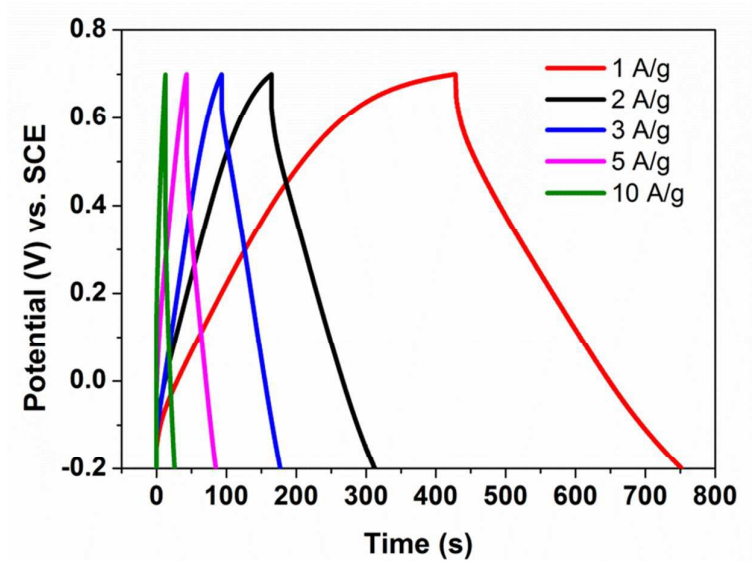


Fig. 7 Galvanostatic charge/discharge curves obtained for CNF@G/PPy core-shell electrode at different current densities.

Electrochemical impedance studies (EIS) were conducted to understand the interaction between graphene and PPy. Nyquist plots of the CNF@PPy and CNF@G/PPy core-shell electrodes are shown in Fig. 8. The intercept of the arc at the real axis in the high frequency region corresponds to the equivalent series resistance (ESR), which is attributed to the resistance of the electrolyte; the intrinsic resistance of the active materials; and the contact resistance between the electrolyte, active materials, and current collector. The charge transfer resistance (R_{ct}) can be determined from the diameter of the arc.⁴⁶ The CNF shows the lowest ESR value (3.3 Ω) with no

evident of a semicircle, indicating a negligible charge transfer resistance due to the absence of electro-active material. This shows that CNF is a suitable candidate to be used as a conductive network where the core-shell layer can be easily accessed to the electrolyte ions, maximizing the utilization of the active material. From the Nyquist plot, the ESR values are determined to be 5.3, 4.1, 4.0 and 3.8 Ω for the CNF@PPy and the CNF@G/PPy with the 0.1 M to 0.3 M pyrrole monomer, respectively. The decrease in the ESR values of the G/PPy composites compared to that of a pure PPy electrode validates the reduction process of the nonconductive GO to conductive graphene during the electrodeposition process.⁴⁷ The crucial role of graphene can be clearly seen by comparing the R_{ct} values of the electrodes. The R_{ct} values of the CNF@PPy and CNF@G/PPy with the 0.1 M to 0.3 M solutions were calculated to be 13.5, 9.3, 5.1, and 6.3 Ω , respectively. The R_{ct} values for the CNF@G/PPy core-shell electrodes were all lower than that for the CNF@PPy electrode because of the incorporation of graphene into the PPy matrix. This also proved that GO had been successfully reduced to graphene during the electrodeposition process as EIS technique had been explored by Casero et al. to discern GO from graphene where GO is known to be a nonconductive material with high R_{ct} value.⁴⁸ Furthermore, the increased conductivity caused by graphene in the composite reduces the distance for electron shuttling and interchain hopping along the PPy conjugated chains and thus improved the overall conductivity for faster electron transport during electrochemical reactions.^{49,50} The CNF@G/PPy-0.2M electrode possesses the lowest R_{ct} value, indicating a faster Faradic reaction and ideal capacitive behaviour, which is in agreement with the CV and GCD results. This also confirms that 0.2 M of the pyrrole monomer is the optimum concentration for the electrodeposition for CNF@G/PPy electrode, enhancing the effectiveness of both the graphene and PPy and attaining the maximum electrochemical performance. At a low frequency region, all of the electrodes have vertical lines close to 90° indicating the low diffusion resistance of the electrolyte ions in the electrode structure, which shows the good porous structure and high specific surface area of the CNF support.^{39,51}

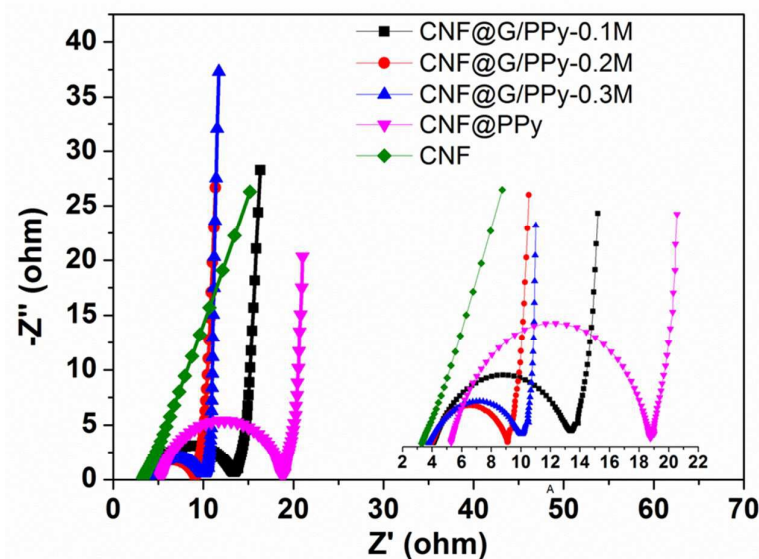


Fig. 8 Nyquist plots of EIS for CNF substrate, CNF@PPy and CNF@G/PPy core-shell electrodes. Inset is the magnified portion of the high-frequency region.

4. Conclusion

In summary, a graphene/PPy composite was successfully electrodeposited on a CNF substrate using GO and pyrrole as the starting materials. The in-situ polymerization of PPy and the reduction of GO gave rise to a three-dimensional interconnected framework with a core-shell structure that made the electrode materials more accessible to the electrolyte. This unique structure was the reason that the CNF@G/PPy core-shell electrode outperformed its graphene-free counterpart. The optimum concentration for the pyrrole monomer was found to be 0.2 M and it showed a specific capacitance of 386 F/g at 2 mV/s. The introduction of graphene improved the electrical conductivity and electrochemical properties of PPy, allowing the core-shell electrode to operate at a current density as high as 10 A/g with reasonable capacitance retention. Graphene also enhanced the electrochemical stability and rate performances of the PPy, retaining 84% of its initial capacitance value for 1000 charge/discharge cycles. Considering the advantages of G/PPy and its facile preparation, the CNF@G/PPy core-shell electrode is a promising material for high performance supercapacitors.

Acknowledgements

The authors gratefully acknowledge the financial support by University of Malaya Research Grant UMRG Programme (RP007C-13AFR); the Science Fund from the Ministry of Science, Technology and Innovation (06-01-04-SF1513); High Impact Research Grant from the Ministry of Higher Education of Malaysia (UM.C/625/1/HIR/MOHE/05).; and TWAS Research Grants.

References

1. P. Simon and Y. Gogotsi, *Nat. Mater.*, 2008, **7**, 845–854.
2. G. Yu, L. Hu, M. Vosgueritchian, H. Wang, X. Xie, J. R. McDonough, X. Cui, Y. Cui, and Z. Bao, *Nano Lett.*, 2011, **11**, 2905–2911.
3. L. L. Zhang and X. S. Zhao, *Chem. Soc. Rev.*, 2009, **38**, 2520–2531.
4. S. Chen, J. Zhu, X. Wu, Q. Han, and X. Wang, *ACS Nano*, 2010, **4**, 2822–2830.
5. Q. Li, J. Liu, J. Zou, A. Chunder, Y. Chen, and L. Zhai, *J. Power Sources*, 2011, **196**, 565–572.
6. H. Chang and H. Wu, *Energy Environ. Sci.*, 2013, **6**, 3483–3507.
7. M. D. Stoller, S. Park, Y. Zhu, J. An, and R. S. Ruoff, *Nano Lett.*, 2008, **8**, 3498–3502.
8. M. J. Allen, V. C. Tung, and R. B. Kaner, *Chem. Rev.*, 2010, **110**, 132–145.
9. M. Hughes, G. Z. Chen, M. S. P. Shaffer, D. J. Fray, and A. H. Windle, *Compos. Sci. Technol.*, 2004, **64**, 2325–2331.
10. L. R. Hepowit, K. M. Kim, S. H. Kim, K. S. Ryu, Y. M. Lee, and J. M. Ko, *Polym. Bull.*, 2012, 873–880.
11. G. A. Snook, P. Kao, and A. S. Best, *J. Power Sources*, 2011, **196**, 1–12.
12. E. Frackowiak, V. Khomenko, K. Jurewicz, K. Lota, and F. Béguin, *J. Power Sources*, 2006, **153**, 413–418.
13. H. An, Y. Wang, X. Wang, L. Zheng, X. Wang, L. Yi, L. Bai, and X. Zhang, *J. Power Sources*, 2010, **195**, 6964–6969.
14. B. Muthulakshmi, D. Kalpana, S. Pitchumani, and N. G. Renganathan, *J. Power Sources*, 2006, **158**, 1533–1537.

15. A. Izadi-Najafabadi, D. T. H. Tan, and J. D. Madden, *Synth. Met.*, 2005, **152**, 129–132.
16. J.-H. Kim, Y.-S. Lee, A. K. Sharma, and C. G. Liu, *Electrochim. Acta*, 2006, **52**, 1727–1732.
17. K. Sode, T. Sato, M. Tanaka, Y. Suzuki, and H. Kawakami, *Polym. J.*, 2013, **45**, 1210–1215.
18. J. J. Mack, L. M. Viculis, A. Ali, R. Luoh, G. Yang, H. T. Hahn, F. K. Ko, and R. B. Kaner, *Adv. Mater.*, 2005, **17**, 77–80.
19. W. Nuansing, S. Ninmuang, W. Jareenboon, S. Maensiri, and S. Seraphin, *Mater. Sci. Eng. B*, 2006, **131**, 147–155.
20. M. Inagaki, Y. Yang, and F. Kang, *Adv. Mater.*, 2012, **24**, 2547–2566.
21. A. Ghosh, E. J. Ra, M. Jin, H.-K. Jeong, T. H. Kim, C. Biswas, and Y. H. Lee, *Adv. Funct. Mater.*, 2011, **21**, 2541–2547.
22. L. Zhao, Y. Qiu, J. Yu, X. Deng, and X. Bai, 2013, 4902–4909.
23. Y. Liu, Y. Zhang, G. Ma, Z. Wang, K. Liu, and H. Liu, *Electrochim. Acta*, 2013, **88**, 519–525.
24. J.-G. Wang, Y. Yang, Z.-H. Huang, and F. Kang, *Electrochim. Acta*, 2011, **56**, 9240–9247.
25. A. Liu, C. Li, H. Bai, and G. Shi, *J. Phys. Chem. C*, 2010, **114**, 22783–22789.
26. J. Wang, Y. Xu, J. Zhu, and P. Ren, *J. Power Sources*, 2012, **208**, 138–143.
27. N. M. Huang, H. N. Lim, C. H. Chia, M. a Yarmo, and M. R. Muhamad, *Int. J. Nanomedicine*, 2011, **6**, 3443–3448.
28. M. Hilder, B. Winther-jensen, D. Li, M. Forsyth, and D. R. Macfarlane, *Phys. Chem. Chem. Phys.*, 2011, **12**, 9187–9193.
29. Y. S. Lim, Y. P. Tan, H. N. Lim, N. M. Huang, and W. T. Tan, *J. Polym. Res.*, 2013, **20**, 156.
30. S. Sadki, P. Schottland, G. Sabouraud, and N. Brodie, 2000, 283–293.
31. C. A. Amarnath, C. E. Hong, N. H. Kim, B.-C. Ku, T. Kuila, and J. H. Lee, *Carbon N. Y.*, 2011, **49**, 3497–3502.
32. A. Davies, P. Audette, B. Farrow, F. Hassan, Z. Chen, J.-Y. Choi, and A. Yu, *J. Phys. Chem. C*, 2011, **115**, 17612–17620.
33. S. Y. Kim, B.-H. Kim, K. S. Yang, and K.-Y. Kim, *Mater. Lett.*, 2012, **71**, 74–77.
34. E.-Y. Choi, T. H. Han, J. Hong, J. E. Kim, S. H. Lee, H. W. Kim, and S. O. Kim, *J. Mater. Chem.*, 2010, **20**, 1907–1912.
35. M. Omastová, M. Trchová, J. Kovářová, and J. Stejskal, *Synth. Met.*, 2003, **138**, 447–455.
36. X. Feng, Z. Yan, R. Li, X. Liu, and W. Hou, *Polym. Bull.*, 2013, **70**, 2291–2304.

37. S. P. Lim, N. M. Huang, and H. N. Lim, *Ceram. Int.*, 2013, **39**, 6647–6655.
38. Z. Gu, C. Li, G. Wang, L. Zhang, X. Li, W. Wang, and S. Jin, *J. Polym. Sci. Part B Polym. Phys.*, 2010, **48**, 1329–1335.
39. J.-G. Wang, Y. Yang, Z.-H. Huang, and F. Kang, *J. Mater. Chem.*, 2012, **22**, 16943–16949.
40. M. Zhi, A. Manivannan, F. Meng, and N. Wu, *J. Power Sources*, 2012, **208**, 345–353.
41. J. S. Im, S.-J. Park, T. J. Kim, Y. H. Kim, and Y.-S. Lee, *J. Colloid Interface Sci.*, 2008, **318**, 42–49.
42. S. K. Nataraj, K. S. Yang, and T. M. Aminabhavi, *Prog. Polym. Sci.*, 2012, **37**, 487–513.
43. F. Gong, X. Xu, G. Zhou, and Z.-S. Wang, *Phys. Chem. Chem. Phys.*, 2013, **15**, 546–552.
44. J. Miao, M. Miyauchi, T. J. Simmons, J. S. Dordick, and R. J. Linhardt, *J. Nanosci. Nanotechnol.*, 2010, **10**, 5507–5519.
45. Y. S. Lim, Y. P. Tan, H. N. Lim, N. M. Huang, W. T. Tan, M. A. Yarmo, and C.-Y. Yin, *Ceram. Int.*, 2014, **40**, 3855–3864.
46. Y. Ju, G. Choi, H. Jung, and W. Lee, *Electrochim. Acta*, 2008, **53**, 5796–5803.
47. Y. S. Lim, Y. P. Tan, H. N. Lim, W. T. Tan, M. A. Mahnaz, Z. A. Talib, N. M. Huang, A. Kassim, and M. A. Yarmo, *J. Appl. Polym. Sci.*, 2013, **128**, 224–229.
48. E. Casero, a. M. Parra-Alfambra, M. D. Petit-Domínguez, F. Pariente, E. Lorenzo, and C. Alonso, *Electrochem. commun.*, 2012, **20**, 63–66.
49. Y. Han, B. Ding, and X. Zhang, *Chinese Sci. Bull.*, 2011, **56**, 2846–2852.
50. J. Joo, J. K. Lee, S. Y. Lee, K. S. Jang, E. J. Oh, and A. J. Epstein, *Macromolecules*, 2000, **33**, 5131–5136.
51. W. Yang, Z. Gao, J. Wang, B. Wang, Q. Liu, Z. Li, T. Mann, P. Yang, M. Zhang, and L. Liu, *Electrochim. Acta*, 2012, **69**, 112–119.